China Geology 6 (2023) 269−284

China Geology

Journal homepage: http://chinageology.cgs.cn
https://www.sciencedirect.com/journal/china-geology

Paleomagnetism of late Cretaceous dykes in the Gangdese belt: New constraints on the position and structure of the southern margin of Asia prior to the India-Asia collision

Zhi-yu Yi[a, b,*], Si-lin Yang[a, b], Joseph G. Meert[c], Xu-xuan Ma[d]

[a] *Planetary Environmental and Astrobiological Research Laboratory (PEARL), School of Atmospheric Sciences, Sun Yat-sen University, Zhuhai* 519000, *China*
[b] *Key Laboratory of Tropical Atmosphere-Ocean System, Ministry of Education, Zhuhai* 519082, *China*
[c] *Department of Earth & Planetary Sciences*, 112 *Williamson Hall, University of Florida, Gainesville, FL* 32611, *USA*
[d] *Key Laboratory for Continental Tectonics and Dynamics, Institute of Geology, Chinese Academy of Geological Sciences, Beijing* 100037, *China*

ARTICLE INFO

Article history:
Received 30 August 2022
Received in revised form 29 October 2022
Accepted 15 December 2022
Available online 20 February 2023

Keywords:
Paleomagnetism
Diorite dyke
Granodiorite
India-Asia collision
Southern Tibet
Geological survey engineering
Lhasa Terrane

ABSTRACT

This paper report paleomagnetic data from late Cretaceous diorite dykes that sub-vertically intrude granodiorites in the eastern Gangdese belt near the city of Lhasa. Our research goals are to provide further constraints on pre-collisional structure of the southern margin of Asia and the onset of the India-Asia collision. Magnetite is identified as the main magnetic carrier in our study. The magnetite shows no evidence of metamorphism or alteration as determined from optical and scanning electron microscope observations. A strong mineral orientation is revealed by anisotropy of magnetic susceptibility analysis both for the intruded dykes and the country rocks. The authors interpret this AMS fabric to have formed during intrusion rather than deformation. Fifteen of 23 sites yield acceptable site mean characteristic remanences with dual polarities. A scatter analysis of the virtual geomagnetic poles suggests that the mean result adequately averaged paleosecular variation. The paleomagnetic pole from the Gangdese dykes yields a paleolatitude of 14.3°N±5.8°N for the southern margin of Asia near Lhasa. The paleolatitude corresponds to an in-between position of the Lhasa terrane during about 130–60 Ma. Furthermore, the mean declination of the characteristic remanent magnetization reveals a significant counterclockwise rotation of 18°±9° for the sampling location since about 83 Ma. In the light of tectonic setting of the dykes, the strike of the southern margin of Asia near Lhasa is restored to trend approximately about 310°, which is compatible with the hypothesis that the southern margin of Eurasia had a quasi-linear structure prior to its collision with India.

1. Introduction

The pre-collisional configuration of the southern margin of Asia is an important base for estimating the initial timing of the India-Asia collision along with the magnitude of crustal shortening in Asian interior. The paleogeography can be estimated through the evaluation of late Cretaceous paleomagnetic data from the Lhasa terrane (Zhu XY et al., 1977; Zhu ZW et al., 1981; Pozzi JP et al., 1982; Westphal M et al., 1983; Achache J et al., 1984; Lin JL and Watts DR, 1988; Achache J, 1991; Chen Y et al., 1993; Tan XD et al., 2010; Sun ZM et al., 2012; van Hinsbergen DJ et al., 2012; Lippert PC et al., 2014; Cao Y et al., 2017; Yi ZY et al., 2015; Liang YL et al., 2017; Tong YB et al., 2017, 2022). The Gangdese arc, that approximates the southern margin of Asia, is an ideal target for paleomagnetic studies (Aitchison JC et al., 2007).

There are numerous published paleomagnetic studies from late Cretaceous sedimentary and volcanic rocks in the eastern segment of the Lhasa terrane. Red beds, assigned to the Shexing Formation (the upper unit of the Takena Formation in some older literature), record paleomagnetic inclinations between 16°–40°, corresponding to paleolatitudes between about 8°N–23°N (Zhu XY et al., 1977; Zhu ZW et al., 1981; Pozzi JP et al., 1982; Westphal M et al., 1983; Achache J et al., 1984; Lin JL and Watts DR, 1988; Achache J, 1991; Tan XD et al., 2010; Sun ZM et al., 2012; Cao Y et al., 2017; Liang YL et al., 2017; Tong YB et al., 2017; Ma YM et al., 2022). Previous studies on red beds were used to argue for a

* Corresponding author: *E-mail address*: yizhy5@mail.sysu.edu.cn (Zhi-yu Yi).

Literary editor: Xi-jie Chen
doi:10.31035/cg2022077
2096-5192/© 2023 China Geology Editorial Office.

pre-collisional latitude of about 10°N for the southern margin of Asia (Pozzi JP et al., 1982; Westphal M et al., 1983; Achache J et al., 1984; Achache J, 1991). That paleolatitude determination formed a strong basis for the argument that the initial collision between India and Asia took place at 50–55 Ma (Patriat P and Achache J, 1984). Subsequently, problems with inclination shallowing were recognized in many studies (Tan XD and Kodoma KP, 2002; Tauxe L, 2005). After correcting for inclination shallowing, a higher paleolatitude of about 24°N was considered more viable (Tan XD et al., 2010; Lippert PC et al., 2014). However, red beds suffer from magnetic inclination shallowing that has been proven complicated and controversial (Tong YB et al., 2017). An additional issue arises in these studies with respect to the possibility of pervasive remagnetization of red beds and/or volcanic rocks (Pozzi JP et al., 1982; Huang WT et al., 2015; Liang YL et al., 2017). Paleomagnetic data from the coeval igneous rocks are therefore important for further clarifying the pre-collisional configuration of the southern margin of Asia (Cao Y et al., 2017; Ma YM et al., 2017; Yi ZY et al., 2015, 2021; Tong YB et al., 2022).

Late Cretaceous volcanic rocks are irregularly distributed in the eastern segment of the Lhasa Terrane with exception of a few layers intercalated within the Shexing Formation red beds. Sun ZM et al. (2012) and Tong YB et al. (2022) reported paleomagnetic data from basalt layers intercalated within the uppermost Shexing Formation. From this unit, a set of relatively low inclinations were identified, which corresponds to a paleolatitude of 9.8°±2.7° at about 74–72 Ma. Cao Y et al. (2017) reported paleomagnetic data from a "volcano"-sedimentary succession from the upper Shexing Formation which includes 11 "volcanic" sites. The total of 21 sites yielded a paleolatitude of about 10°N. However, stratigraphic and sedimentological investigations revealed that the "volcanic" layers sampled by Cao Y et al. (2017) are actually igneous sills (Wang JG et al., 2020). Moreover, Tan XD et al. (2010) reported paleomagnetic data from both red beds and lava flows from the lower part of the Shexing Formation, which yielded a paleolatitude of about 24°N for the Lhasa Terrane. The mean characteristic remanences (ChRMs) from the two units differ both in declination and inclination suggesting more complexity than might be explained by inclination shallowing of the red bed results (Yi ZY et al., 2015).

Paleomagnetic data obtained from the Linzizong Group in the Linzhou Basin are also widely used in reconstructing the geometry of the India-Asia collision (Yi ZY et al., 2011; Najman Y et al., 2010; van Hinsbergen DJJ et al., 2012; Lippert PC et al., 2014; Huang WT et al., 2013, 2015; Yi ZY et al., 2021). These data also present some issues of interpretation. Paleomagnetic studies from the upper Linzizong Group (the Pana formation) show wide variations in paleolatitudes ranging between about 10°N to 30°N, probably caused by problems of incomplete averaging of paleosecular variation (PSV) for the volcanic rocks in the lower part (Liebke U et al., 2010) and inclination shallowing within the sedimentary rocks from the upper part (Huang WT et al., 2013). Moreover, due to the relatively young age of the Pana Formation (about 48–44 Ma, Zhou S et al., 2004), the results cannot provide a reliable constraint on the pre-collisional geometry of the southern margin of Asia (Yi ZY et al., 2015).

Chen JS et al. (2010, 2014) obtained a paleolatitude of about 6°N from a collection within the lower part of the Linzizong Group (the Dianzhong Formation). Huang WT et al. (2015) countered that the results of Chen JS et al. (2010, 2014) may have suffered chemical and/or thermal remagnetization. On the positive intraformational conglomerate test along with a re-evaluation of paleomagnetic data from Chen JS et al. (2010, 2014) and Huang WT et al. (2015). Yi ZY et al. (2021) confirmed a primary origin for the Dianzhong Formation in the Linzhou Basin. Yi ZY et al. (2021) further suggested a southward shift of the Lhasa Terrane (more likely, the continent Asia as a whole) prior to the India-Asia collision.

The aforementioned discussion indicates that the paleomagnetic data for the eastern segment of the Lhasa terrane are still unsatisfactory in consideration of the complexity of the shape or kinematics of the southern margin of Asia. In this study, a group of late Cretaceous dioritic dykes and their granodioritic host were selected for a paleomagnetic investigation from the Gangdese belt near the city of Lhasa. The dykes are well insulated from tectonic folding due to the rigidity of the granitic host and thus offer the potential to constrain the paleoposition of the southern margin of Asia prior to its collision with India as well as detail any post-emplacement rotation of the region.

2. Geological setting and paleomagnetic sampling

The tectonic units of the Tibetan plateau are shown in Fig. 1a including the large calc-alkaline composite batholith known as the Gangdese magmatic belt. The Gangdese belt lies along the southern margin of the Lhasa terrane with a width of about 20–60 km and a length of more than 2000 km. The magmatic products in this belt record the subduction history of the Neo-Tethys and the initial India-Asia collision (Chung SL et al., 2005; Ji WQ et al., 2009; Zhu DC et al., 2013; Zhang X et al., 2019). The Gangdese magmatic belt developed over a protracted interval between 237 and 13 Ma (Schärer U and Allbgre CJ, 1984; Ji WQ et al., 2009; Hu XM et al., 2015; Wang C et al., 2016) with 4 dominant magmatic phases at 230–136 Ma, 110–80 Ma, 65–40 Ma and 25–13 Ma (Ji WQ et al., 2009). The late Cretaceous magmatism with "flare-up" character is determined by a spectral analysis of zircon U-Pb ages, probably due to the northward subduction of the Neo-Tethyan oceanic lithosphere (Ji WQ et al., 2009; Guo LS et al., 2011, 2013; Ma L et al., 2013; Xu WC et al., 2015).

Our sampling location near the city of Lhasa is shown in Fig. 1b. A suit of granodiorite plutons with intrusion of diorite dyke is exposed along a road cut at the eastern bank of the Lhasa River near the village of Liandong (Fig. 2b). The geological setting of the sampling region was described in detail by Ma XX et al. (2017). U-Pb isotopic dating yields ages of 82.7±2.7 Ma and 83.5±3.5 Ma for the diorite dykes

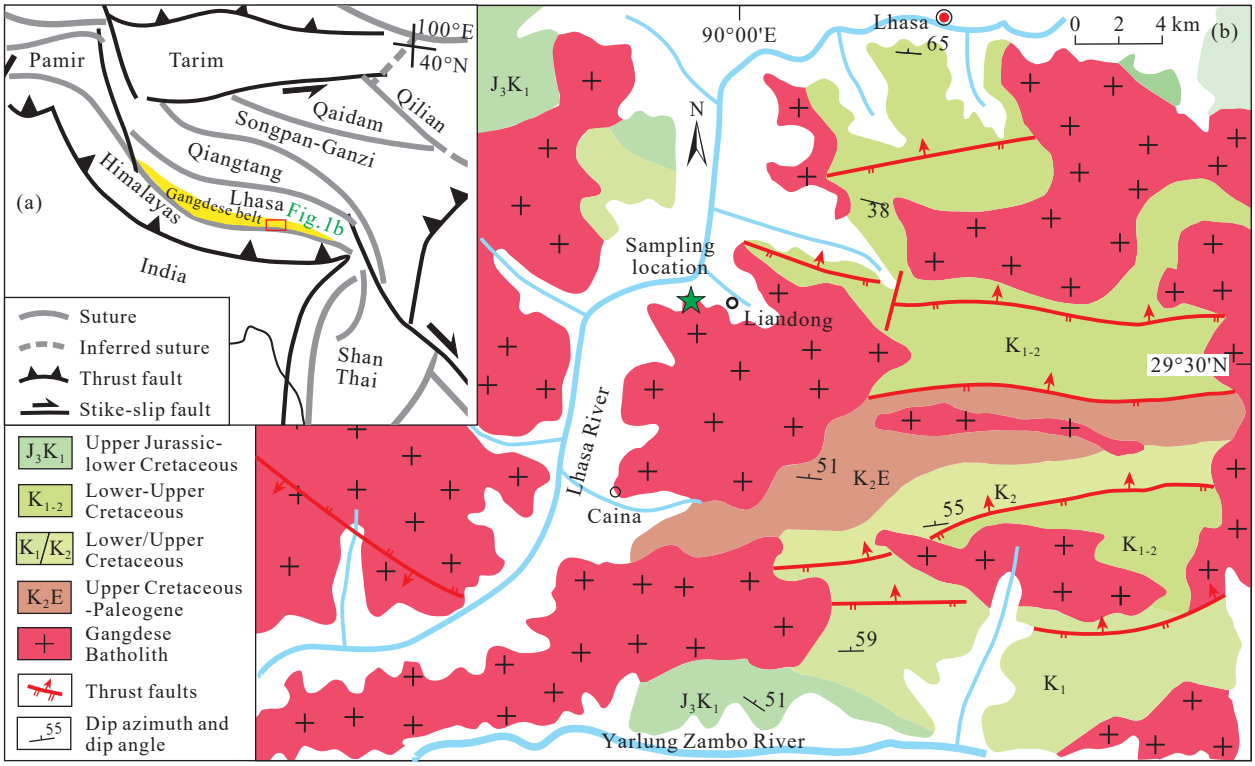

Fig. 1. a–Tectonic framework of the Lhasa Terrane and adjacent area (after Enkin RJ et al., 1991); b–simplified regional geologic map of the Gangdese magmatic arc near Lhasa showing distribution of the Mesozoic and Cenozoic rock units and paleomagnetic sampling locations.

and 85.8±1.7 Ma and 86.4±1.1 Ma for the country rocks, respectively (Ma XX et al., 2017). Magma flow structure is a notable feature for the dykes and country rock that can be observed both in the outcrop and thin-section levels (Ma XX et al., 2017). Intensive magma mixing is identified near the boundary between the dykes and country rocks, suggesting that the host rock had not completely solidified during the intrusion of dykes (Ma XX et al., 2017).

The diorite dykes range in width between 0.3–4.0 m and are tilted to the south with dip angles of about 70° (Figs. 2a, c). 23 sites were collected including 22 diorite dykes and one host rock site. Generally, 10–12 paleomagnetic samples were collected from each site by a portable gasoline-powered drill and oriented in situ by both magnetic and sun compasses. Orientations measured by the two compasses are consistent.

3. Methods

Core samples were cut into one or two standard cylindrical specimens (2.5 cm × 2.2 cm). Some fresh end material was further processed into thin sections for microscopic observation, or ground into powder for rock magnetic analysis.

In an effort to identify the nature of magnetic minerals, pilot specimens were selected from both the dykes and country rock for scanning electron microscope (SEM) and light microscope observations. Rock magnetic experiments were conducted along with the microscopy to further characterize the composition and domain state of the magnetic carriers. Rock magnetic experiments were conducted on a Princeton/MicroMag 3900 Vibrating Sample Magnetometer (VSM). Hysteresis loops and Hcr were measured at room temperature with a field range of ±0.4 T to ±1 T and FORC diagrams were measured with δB = 2.3 mT and calculated with SF = 7. In an effort to identify magnetic fabrics within the plutonic rocks, anisotropy of magnetic susceptibility (AMS) of 202 specimens from 23 sites was measured using a KLY-4 kappabridge. A total of 240 standard core specimens were subjected to progressive thermal demagnetization using a Schonstedt oven with residual magnetic field minimized to less than 10 nT inside the cooling chamber. Demagnetization was performed at 12–15 successive steps with intervals of 50°C or 100°C to 500°C, subsequently reduced to 20°C or 10°C as the maximum unblocking temperatures of about 580°C were approached. Magnetic remanence was measured with a 2G 3-axis cryogenic magnetometer. All demagnetization treatments and remanence measurements were performed in a magnetically shielded room with residual fields less than 300 nT at the laboratory of paleomagnetism at South China Sea Institute of Oceanology, Chinese Academy of Sciences.

Demagnetization results were evaluated using stereographic projections and orthogonal diagrams (Zijderveld JDA, 1967). Most specimen directions were determined using principal component analysis (Kirschvink JL, 1980) to obtain line-fits of ChRM from at least four successive steps, whilst five of the total were derived from the best fit to remagnetization great circles (Halls HC, 1978). Site mean directions were calculated using the ChRMs with maximum angular deviations (MADs) less than 10°, and sample directions greater than two standard deviations away from the mean direction were excluded at site level. The site-mean ChRM directions and VGP averaging (to calculate a

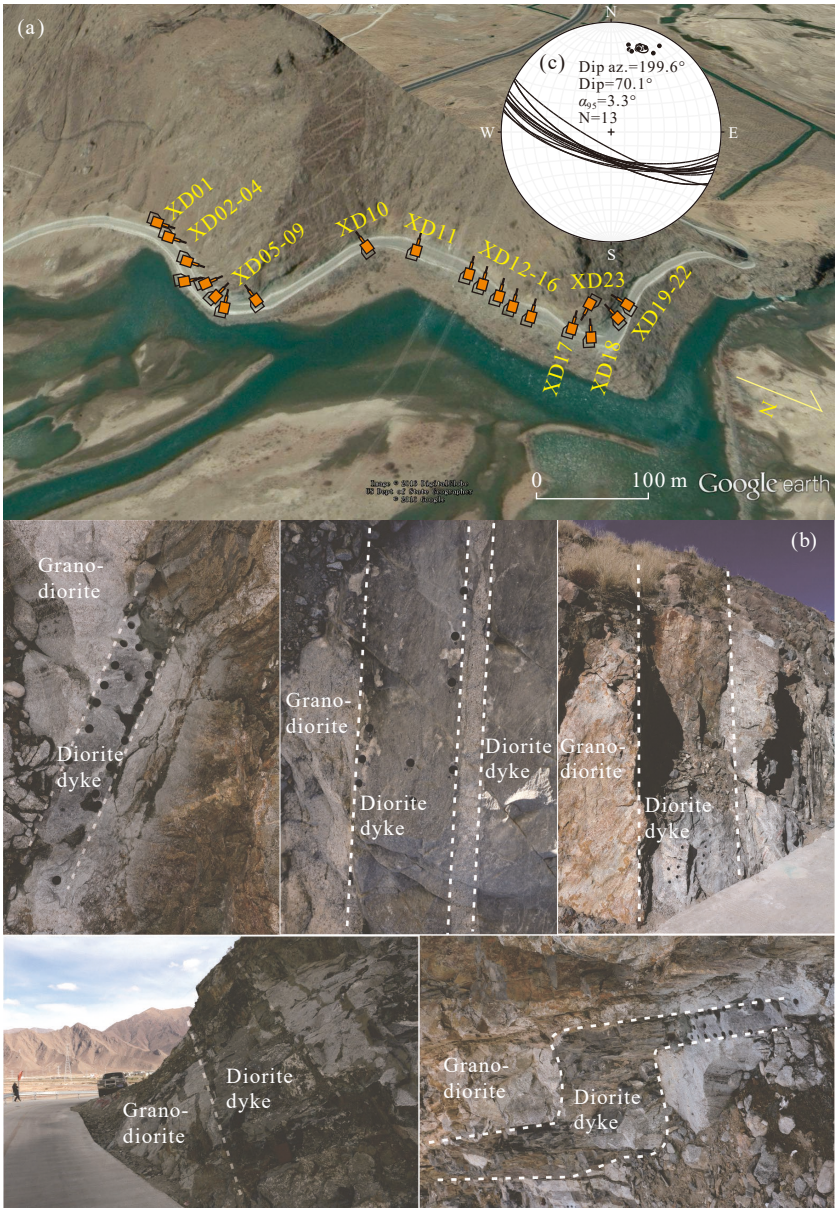

Fig. 2. Field photos showing distribution of the sampling sites (b) and contacts between the diorite dykes and the country rock (a); plot of the bedding attitutes of sampled diorite dykes (c).

paleomagnetic pole) were determined using the standard Fisherian method (Fisher R, 1953) and spherical statistics was performed with paleomagnetic software PMGSC (version 4.2) offered by R. Enkin.

4. Results

4.1. Petrography

In addition to main minerals such as plagioclase, hornblende and biotite, magnetite (or titanomagnetite) is presented in the thin- and polished rock sections of the pilot samples as accessory mineral (Fig. 3). Energy spectrum analyses (red dots in Figs. 3b, d) indicate a 100% content of iron oxides suggesting that magnetite is the main magnetic carrier for the pilot samples. The intergrowth of magnetite with other minerals (such as amphibole, biotite) indicates an original magmatic texture that was not subjected to subsequent weathering and/or chemical alteration. SEM images of the dyke samples indicate a preferred mineral orientation that the authors interpret as a result of primary magma flow rather than deformation (Fig. 3d).

4.2. Rock magnetism

4.2.1. Anisotropy of magnetic susceptibility (AMS)

The susceptibility varies from 1.0×10^{-3} SI to 1.0×10^{-1} SI. The degree of anisotropy (P_j) is high, ranging from 1.05 to 1.80 with an average of 1.30 (Fig. 4c). The diorite dykes exhibit higher susceptibilities reflecting a higher content of magnetite (Fig. 4c). There are two possible explanations for the relatively high Pj in the dyke samples: 1) the intrusion of dykes was confined to a narrow conduit and hence developed a strong magmatic flow fabric; and/or 2) the diorite dykes have higher content of hornblende (30% in dykes versus

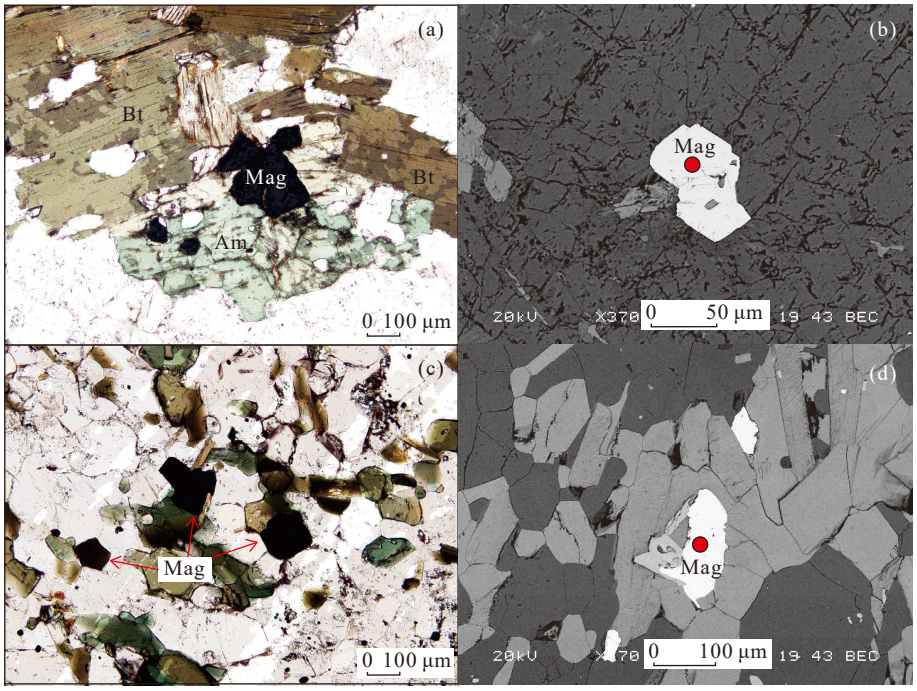

Fig. 3. Optical petrography (a, c) and scanning electron microscope (SEM) observations (b, d) on the thin sections from the diorite dykes (c, d) and granodiorite country rock (a, b) indicate the magnetic minerals are magnetite or titanomagnetite which have not experienced visible alteration. Mineral orientation with insignificant deformation can be observed in (d). Abbreviations: Mag–Magnetite. See text for more information.

5%–10% in the host, Ma XX et al., 2017) and the parallel alignment of which may result in higher Pj (Borradaile CJ and Jackson M, 2004). The AMS shape factors (T) for dyke samples are more oblate as compared to the prolate shape from the country rock (Fig. 4d). The maximum principal ellipsoid axes (K_{max}) distribute along the dyke plane in geographic coordinate system with minimum axes (K_{min}) perpendicular to the plane (Fig. 4a). The average dip of the K_{max} of 63.7°±12.1° before tilt correction is insignificantly different from the mean dip angle of the dykes (about 70°) (Fig. 4a). The authors interpreted the high P_j as a fluid (magma) flow fabric imposed during the emplacement of dykes.

4.2.2. Hysteresis loops, IRM & back-field curves and FORC diagram

Application of magnetic fields during hysteresis studies show that complete saturation is reached before 0.3 Tesla (T) with remanence coercivity (Hcr) less than tens of milliTesla (mT) indicating that these samples are dominated by low-coercivity ferromagnetic phase (Figs. 5a–h). Pilot samples plot within the pseudo-single domain range on a Day diagram (Fig. 5i; Day R et al., 1977; Dunlop DJ, 2002). First order reversal curve (FORC) measurements produced characteristic contours that diverge away from the origin with considerable vertical spread of Hu up to 60 mT, indicating that the magnetic particles are dominantly larger PSD or multiple domain (MD) grains (Roberts AP et al., 2000; Carvallo C et al., 2005; Muxworthy AR and Roberts RP, 2007).

4.3. Field relationships & paleomagnetism

Paleomagnetic studies require detailed knowledge of any structural complexity before making any tectonic interpretation. In mafic dykes studies, there is a common assumption that the dykes were emplaced vertically into the host rocks with some negligible deviations (i.e., within <10 degrees, Buchan KL and Halls HC, 1990; Halls HC et al., 2000; Belica ME et al., 2014). The vertical intrusion model is supported by numerical modelling for the sheeted dykes in the spreading center of a mid-ocean ridge (Liu Z and Burk WR, 2021). When the cold lithosphere deforms in an elastic manner with negligible viscous flow, extensional stresses are generated by the separation of two blocks and a vertical dyke can open (Liu Z and Burk WR, 2021). In tectonically complex regions, these assumptions may not be valid and/or require a more complex solution to determine the original orientation that includes documenting any vertical axis rotations (Morris A and Maffione M, 2016). If dykes intrude into sedimentary or volcanic rocks, the bedding of the host rocks can sometimes be used for structural correction (Chen Y et al., 2004; Liebke U et al., 2010). This study apply the following arguments in assessing the original orientation of the dykes and host rocks in this study.

There are several key field, AMS, microscopic and geochronologic data that the authors use to make an accurate structural correction. First, all 22 sampled dykes, along with a number of unsampled dykes, have very similar structural orientations. The group of dykes were formed in an extension setting (Ma XX et al., 2017) with occurrence similar to sheeted dykes that generally intrude vertically. The dykes are uniformly tilted to the south with dip angles of about 70° and dip azimuths approximately perpendicular to the regional faults (Figs. 1b, 2b). This indicates that the tilting of dykes is likely related to the regional compressive tectonics in the

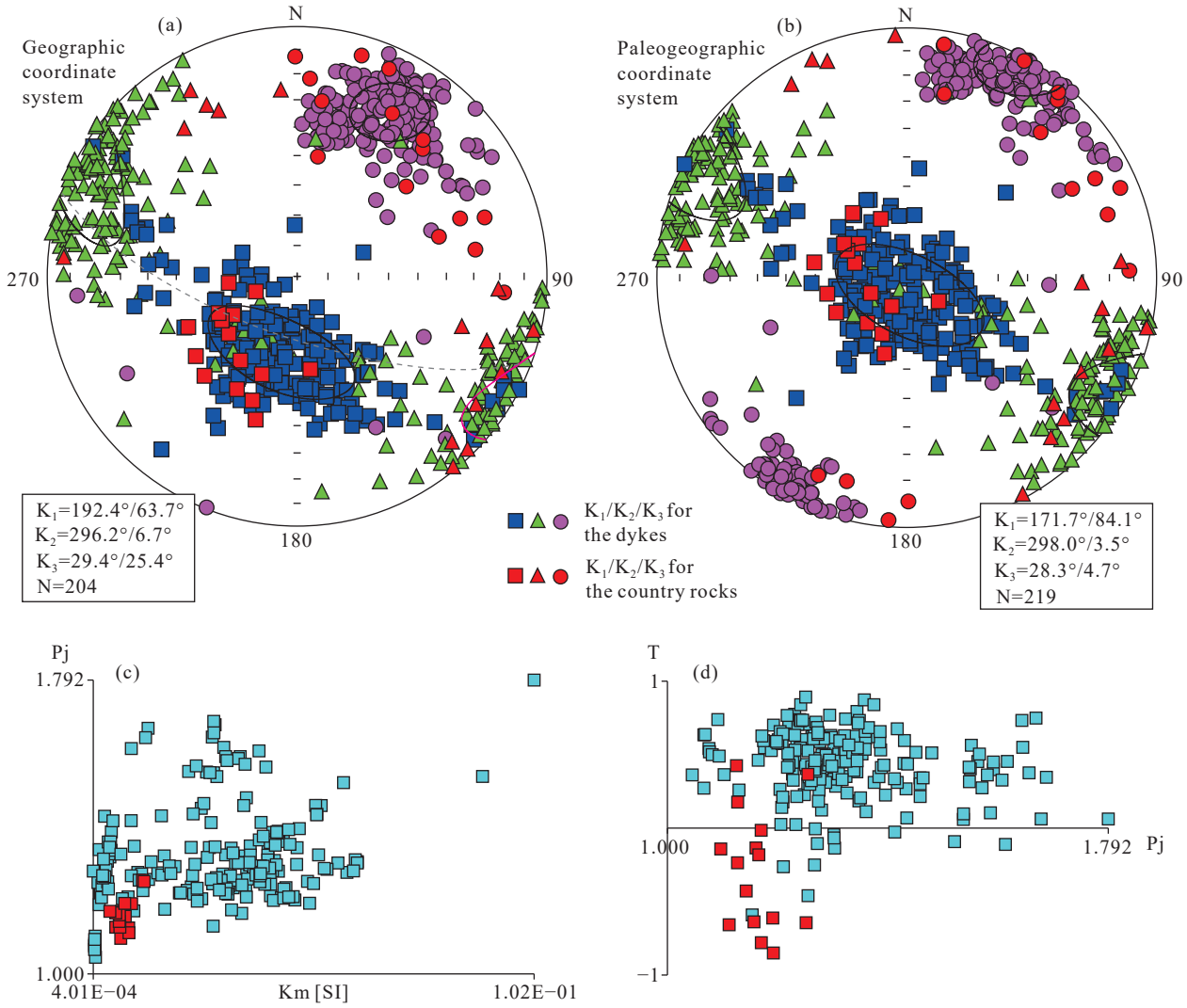

Fig. 4. Stereoplots of three principal axes of anisotropy of magnetic susceptibility (AMS) ellipsoid in geographic (a) and paleogeographic (b) systems and plots of AMS degree (P_j) versus total susceptibility (c) and AMS shape (T) (d) respectively. The pilot samples marked with red color are from granodiorite country rocks and the others are from dykes; the grey dashed arc in (a) represents the mean bedding plane of the dykes.

North-south direction. By adjusting the normal of the dyke to horizontal along a vertical plane, the dykes were restored to be vertical. As a result, the AMS data show that Kmax aligns vertically after the tilt correction, indicating a uniformly vertical intrusion of the dykes that is similar with the intrusion model of sheeted dykes (Fig. 4b; Liu Z and Burk WR, 2021). The vertical intrusion model for the dioritic dykes is supported by the microstructures and geochronologic data of the dykes and the host granites. Ma XX et al. (2017) noted evidence for widespread magma mixing along the margin between the dykes and the host rocks at the outcrop and thin-section level. Ma XX et al. (2017) argued that the host rock had not yet solidified completely during intrusion of the dykes. This is confirmed by our field observations demonstrating that the orientation of the dykes is discordant with brittle features such as joints (Fig. 2a). Magma mixing is further supported by overlapping isotopic ages, similar mineral assemblages and Sr isotopic composition for the dykes and hosts (Ma XX et al., 2017). Furthermore, the ChRMs of the country rock are indistinguishable from the mean direction of the dykes (see the next paragraph) suggesting that both acquired their remanence at the same time as would be expected given their overlapping ages. In the case of magma mixing, any intrusion that deviates significantly from the vertical direction will result in an expanded magma mixing beyond the contact between the dykes and unsolidified hosts, which is obviously at odds with our field observations (Fig. 2a). In consideration of above, the tilt-corrected ChRMs as described below are applied to our tectonic interpretation.

After removal of a low-temperature component by about 250–300°C, 209 out of 240 demagnetized specimens yield acceptable ChRMs generally determined in the temperature interval of about 300–580°C (Figs. 6a–f, Table S1). Some demagnetization trajectories show a hard-shouldered decay near about 580°C (Figs. 6b, e). A total of 14 out of 22 sites from the diorite dykes yield acceptable site-mean ChRM directions with a mean direction of D = 330.4°, I = 42.1°,

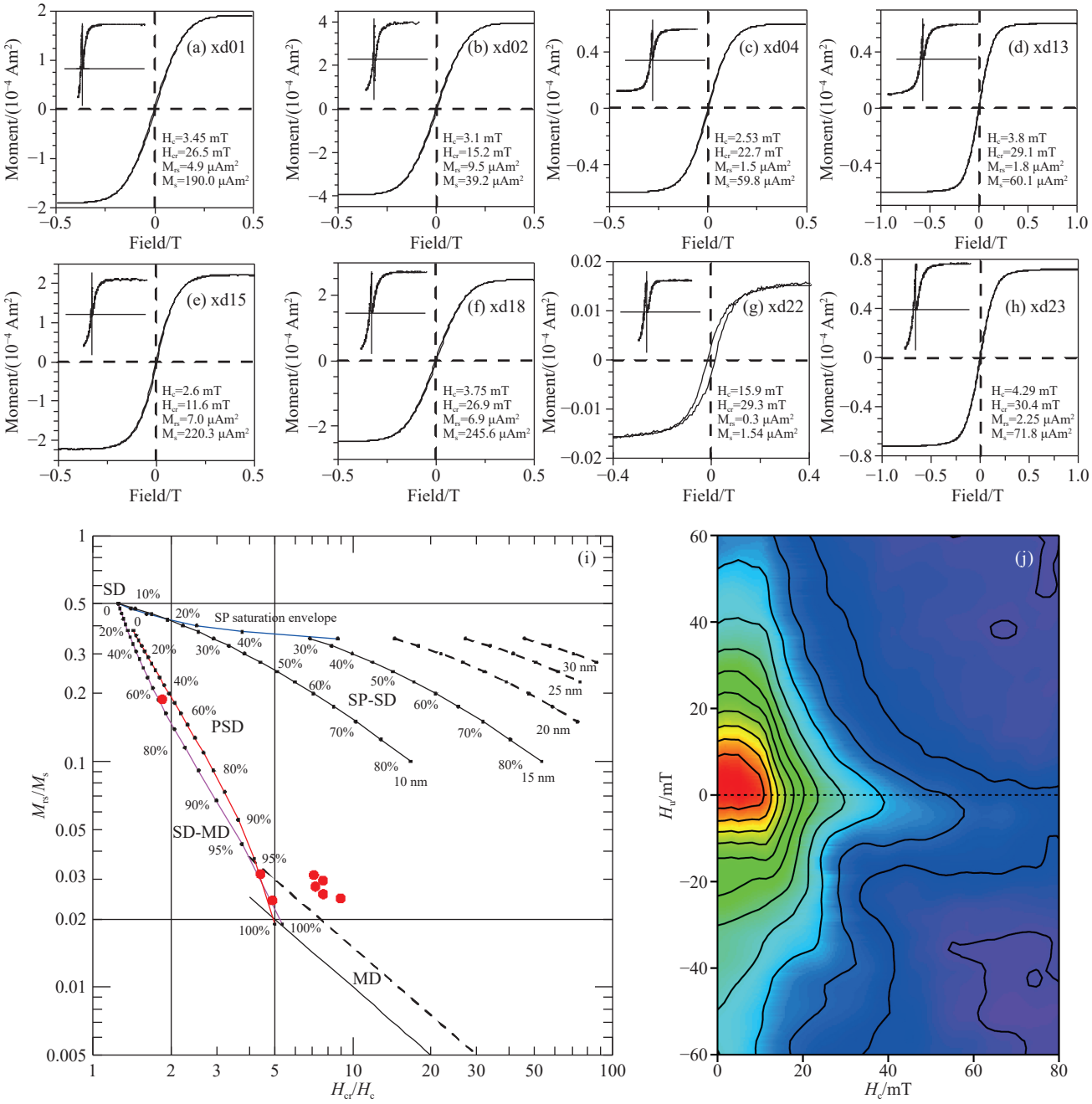

Fig. 5. Representative results of hysteresis loops of the pilot samples from the diorite dykes (a–g) and granodiorite country rock (h) with maximum field of 0.4 to 1.0 Tesla. Acquisition of isothermal remanent magnetization (IRM), back-field demagnetization curves (in the second quadrant of each diagram) with maximum fields of 0.5 T. (i) Day plot (Day R et al., 1977; Dunlop DJ, 2002) of hysteretic parameters calculated from (a–h) showing magnetic particles are plotted within the pseudo-single domain (PSD) range; (j) Representative FORC measurement showing magnetic particles are dominant by larger PSD or MD particles, see text for more explanation.

(α_{95}= 8.1°) before and D = 340.7°, I = 26.8°, (α_{95} = 7.9°) after tilt correction (Table 1). A site from the host granodiorite yields a site mean direction of D = 338.4°, I = 50.5° before and D = 349.0°, I = 29.5°, (α_{95} = 8.5°) after tilt correction (Table 1). The tilt-corrected mean direction obtained from the dyke sites is insignificantly different from the site mean direction obtained from the host rocks with angular difference of 6.5°±8.5°. Combining the total 15 sites yields group mean direction of D = 330.9°, I = 42.7°, (α_{95} = 7.6°) before and D = 341.0°, I = 27.8°, (α_{95} = 7.4°) after tilt correction (Figs. 7a, b, Table 1). For the remaining eight sites, xd05 and xd20 were excluded for larger α_{95} (>15); xd06, xd07, xd12, xd14 were excluded for the insufficient statistical sampling (n<5); and xd14, xd20 were excluded for significant deviation from the mean direction (Figs. 7a, b, Table 1). Although there is slight improvement in grouping for mean ChRM 's in the tilt-corrected data, the fold test performed on the site-mean ChRMs is not statistically significant. Both Normal and reverse polarities have been identified. The McFadden PL and McElhinny MW (1990) 's reversal test is inapplicable at the site level because only one site (XD22) yielded an exclusively reverse polarity. At the specimen level, the angular difference

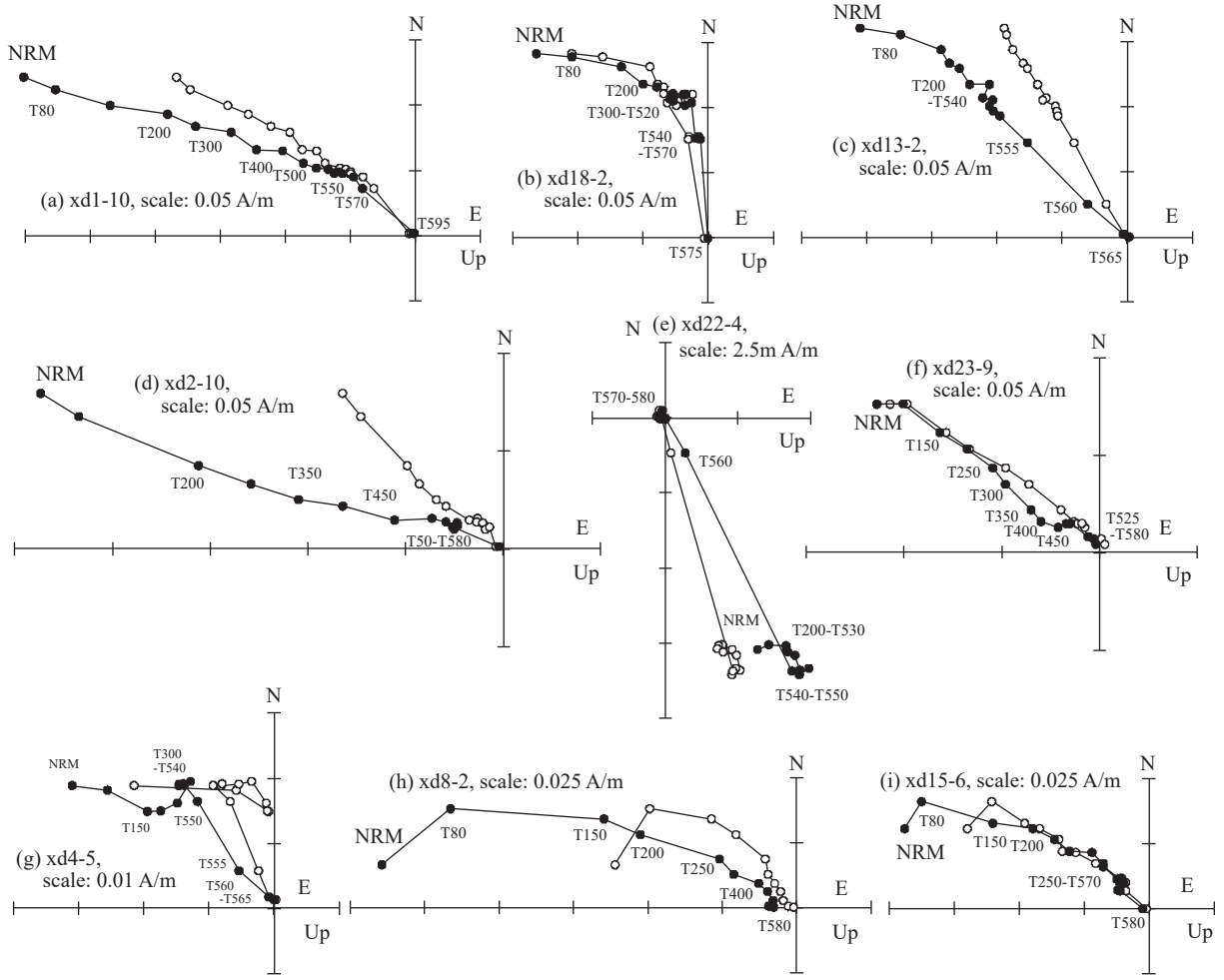

Fig. 6. Orthogonal (Zijderveld) vector plots of representative specimens from the dykes (a–e, g–i) and the country rock (f). Directions are plotted in-situ; open and solid circles represent vectors and endpoints projected onto horizontal and vertical planes, respectively.

of 15.5°±9.0° between the two polarities is large than the critical angle of 9.1°. However, considering that 9/15 reverse ChRMs are mainly from site XD22, the slight deviation is likely caused by inadequate PSV samplin.

5. Discussions

5.1. Reliability

5.1.1. The age of the remanences

The fresh, euhedral magnetite, which is large PSD or MD in size, together with the dual polarities for the ChRMs suggest that the ChRM's are likely primary. This study hence interpret that the ChRM 's were acquired during the emplacement of the pluton. Two groups of zircon U-Pb ages are reported by Ma XX et al. (2017), and they are 85.8±1.7 Ma and 86.4±1.1 Ma for the granodiorite host, and 82.7±2.6 Ma and 83.5±3.5 Ma for the diorite dykes, respectively. This study interpret the crystallization ages as the age of remanence although the cooling age of the pluton would require further thermochronological data.

5.1.2. Paleosecular variation

The assumption of GAD model for the Earth's magnetic field requires the averaging of PSV (Johnson CL et al., 2008). The presence of both normal and reverse polarities in the diorite dykes (Fig. 8; Table 1) suggests that the intrusion or cooling of the dykes occurred over a protracted interval of time (Zhu RX et al., 1994). The VGP scatter (S) of the paleomagnetic pole is 13.1°, which is slightly higher than the predicted value (S=about 10°) for the Cretaceous Normal Superchron (CNS, about 120–84 Ma) (Biggin AJ et al., 2008) but is comparable with that observed over the past 5 Ma (S=about 13°; Johnson CL et al., 2008) at a latitude of about 14°N (Fig. 8). This study suggest that the PSV was properly averaged.

5.2. Paleoposition of the Lhasa Terrane

Statistical averaging of the VGPs obtained from the dykes and country rocks yields a paleomagnetic pole at 67.1°N, 325.1°E with A_{95}=5.8° (Table 1). Our pole predicts a paleolatitude of 14.3°N±5.8°N for the Lhasa terrane at about 83 Ma (at reference site of 91°E, 29°N) which can be used to constrain the paleoposition of the southern margin of Asia prior to its collision with India.

Our tilt-corrected result agrees well with two studies on red beds from the Shexing Formation in the Linzhou basin

Table 1. Site-mean ChRM directions of late Cretaceous dykes (about 83 Ma) from the Gangdese Belt, South Tibet, China.

Site ID	Lithology	Strike/Dip (°)	n/n_0	R/N	Dg(°)	Ig (°)	*Ds* (°)	*Is* (°)	*k*	α_{95} (°)	VGPs	
											Long. (°E)	Lat. (°N)
xd01	Diorite dyke	298/20	7/10	2/5	304.0	51.5	325.9	45.5	28.4	11.5	4.6	60.0
xd02	Diorite dyke	298/20	11/10	0/11	314.2	41.3	328.4	33.3	37.7	7.5	346.7	59.1
xd03	Diorite dyke	298/20	7/8	0/9	337.0	48.9	349.7	34.5	25.1	12.3	315.0	75.9
xd04	Diorite dyke	297/19	12/13	0/12	338.0	36.7	344.2	21.3	87.1	4.8	312.8	66.4
xd05[a]	Diorite dyke	292/23	10/14	0/10	324.0	7.5	324.4	−5.2	3.2	32.5	323.9	43.2
xd06[b]	Diorite dyke	281/20	/11	–	–	–	–	–	–	–	–	–
xd07[b]	Diorite dyke	281/20	/9	–	–	–	–	–	–	–	–	–
xd08	Diorite dyke	287/22	8/11	0/8	333.3	48.9	344.8	31.3	26.8	10.9	322.2	71.2
xd09	Diorite dyke	282/24	7/10	0/7	328.6	52.3	342.2	32.9	35.7	10.2	329.5	70.1
xd10	Diorite dyke	282/24	10/13	0/10	317.4	44.0	331.9	33.4	24.1	10.0	343.6	62.1
xd11	Diorite dyke	282/24	10/15	0/10	306.8	46.0	323.5	32.6	23.7	10.1	349.8	54.7
xd12[b]	Diorite dyke	296/20	/8	–	–	–	–	–	–	–	–	–
xd13	Diorite dyke	296/20	7/8	0/7	331.4	39.8	341.5	26.7	60.3	7.8	323.0	67.0
xd14[c]	Diorite dyke	292/20	5/10	0/5	10.4	−26.3	6.8	−46.4	141.9	6.4	263.9	32.4
xd15	Diorite dyke	296/20	9/11	0/9	325.5	31.8	333.8	20.6	32.3	9.2	328.8	59.1
xd16	Diorite dyke	282/25	5/8	0/5	321.9	59.5	341.4	40.0	50.3	10.9	343.3	72.0
xd17	Diorite dyke	283/25	5/14	3/2	355.9	22.9	357.3	−1.2	55.3	10.4	276.4	59.8
xd18	Diorite dyke	287/20	10/12	1/9	342.5	20.7	344.9	4.1	24.3	10.0	301.4	59.0
xd19[a]	Diorite dyke	288/18	8/11	0/8	332.8	−20.8	325.9	−32.8	5.3	26.6	310.2	32.3
xd20[c]	Diorite dyke	288/21	7/10	0/7	324.8	−14.8	318.1	−26.5	43.3	9.3	319.9	30.6
xd21[b]	Diorite dyke	299/11	/11	–	–	–	–	–	–	–	–	–
xd22	Diorite dyke	292/18	9/12	9/0	169.2	−30.5	173.1	−15.0	82.4	5.7	108.9	−67.2
xd23	Granodiorite(host)	285/24	9/18	0/9	338.4	50.5	349.0	29.5	37.4	8.5	309.8	73.0
Group-mean without xd23			14/23		330.4	42.1			25.1	8.1	326.0	66.6
							340.7	26.8	26.0	7.9	K=42.7, A_{95}=6.2	
Group-mean with xd23			15/23		330.9	42.7			26.3	7.6	325.1	67.1
							341.0	27.8	27.5	7.4	K=44.5, A_{95}=5.8	

Reversal test (McFadden PL and McElhinny MW, 1990): the angular difference of 16.8° between the normal and reversed polarities is less than the critical angle of 30.8° indicative of a positive reversal test of C class.

Abbreviations: Site ID, Site identification; Strike/Dip, strike azimuth and coangle of dip of dyke; n/n_0, number of samples or sites used in calculation/yielded well-defined ChRM or demagnetized; Dg and Ig (Ds and Is), declination and inclination of *in situ* (after tilt-corrected) direction. κ and α_{95}, precision parameter and 95% confidence limit of Fisher statistics; Plat and Plong, latitude and longitude of virtual geomagnetic pole (VGP) in stratigraphic coordinates; K and A_{95}, precision parameter and 95% confidence limit of Fisher statistics for locality-mean VGP.

[a] Site-mean directions discarded for α_{95} >15.

[b] Statistically meaningful results unavailable.

[c] Site-mean directions discarded for significant deviation from the group mean direction, see text for more information.

that recorded primary remanences and yielded paleolatitudes of about 10°N–15°N (Cao Y et al., 2017; Ma YM et al., 2022). In addition, one study focused on two limbs from an anticline near Pengbo where a syn-folding magnetization was identified to occur during the Late Cretaceous (Liang YL et al., 2017). Gradual unfolding analysis, at about 69% when the K_{max} is reached, yielded a mean direction of D = 339.1°, I = 27.3° with α_{95}= 4.1° and a corresponding paleomagnetic pole located at 65.4°N, 327.5°E with A_{95}=3.5°. That paleopole is insignificantly different from the one obtained in this study, and yields a paleolatitude of 13.9°N±3.5°N for the southern margin of the Lhasa Terrane (at reference site of 91°E, 29°N) during the Late Cretaceous. Our result differs from the paleolatitude reported from intercalated lava flows in the Shexing Formation. Considering the magnetic declination discrepancy of about 30° between the red bed and lava flow, this study suggests that the age of magnetization for these two units might be different. The authors discard the paleolatitude determination of Tan XD et al. (2010) for further consideration.

When this study compare our results with those from the Linzizong regions, the estimated paleolatitude in this study agrees with that of the Nianbo Formation (60–52 Ma). This study calculated a mean paleolatitude of 11.1°N±5.3°N on the basis of consistent paleopoles reported by Chen JS et al. (2010, 2014), Liebke U et al. (2010) and Sun ZM et al. (2010) from the Linzhou Basin. The mean paleolatitude is slightly higher than the mean paleolatitude from the Dianzhong Formation (6.7°N±4.4°N at 64–60 Ma, Yi ZY et al., 2021). If the latitudinal discrepancy of about 6–8° does exist between the late Cretaceous and earliest Paleogene results, it means there was a slight southward displacement of the Lhasa terrane during the late Cretaceous to early Paleogene as suggested by Yi ZY et al. (2021).

5.3. The initial collision time between India and Asia

The timing and position of the initial collision between

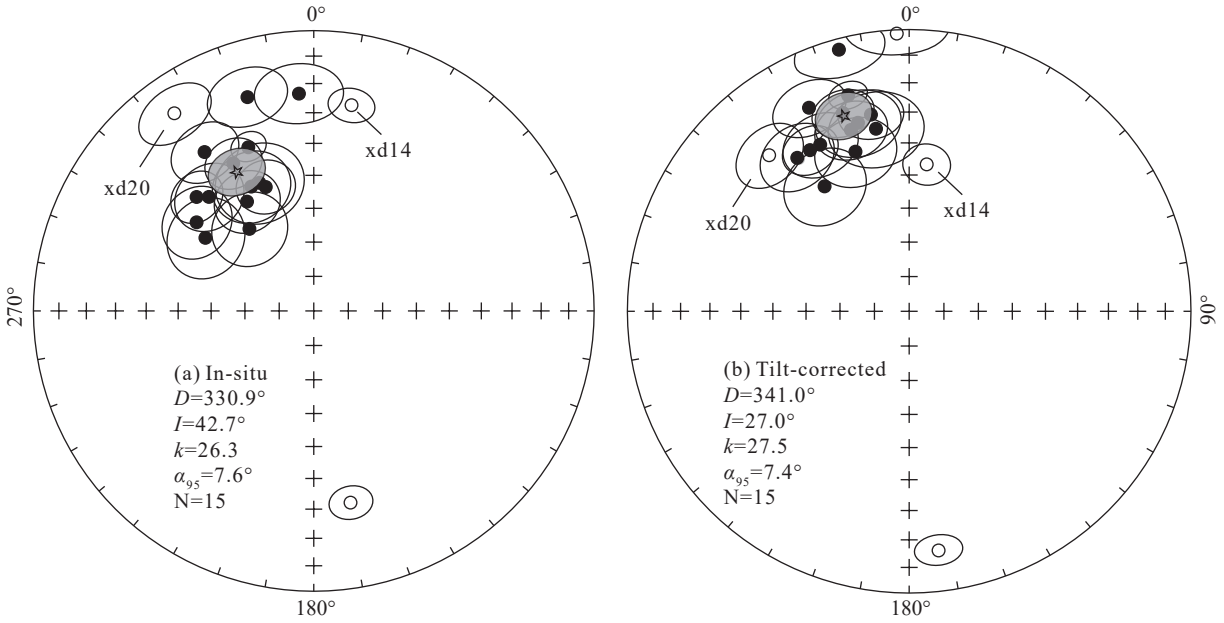

Fig. 7. Equal-area projections of site-mean directions of the ChRMs before and after tilt-correction for the diorite dykes and granodiorite country rocks from the Gangdese Belt, southern Tibet. Solid/open symbols represent downward/upward inclinations; stars indicate the overall mean directions with 95% confidence limits.

India and Asia is evaluated by comparing the paleolatitudinal variations of the Lhasa and Tethyan Himalayan terranes (Table 2). For the position of Asia, this study consider two different scenarios. The first scenario assuming the Lhasa terrane was stationary during the Late Cretaceous. In this case, this paper place the southern margin of Asia at 14.3°N±5.8°N, as constrained by our Gangdese dyke pole. The other scenario is to assume a southward shift of the Lhasa terrane during the Late Cretaceous (more likely, the continental Asia), as suggested by Yi ZY et al. (2021). In this case, this study place the southern margin of Asia at 14.3°N±5.8°N at about 83 Ma and 6.7°N±4.4°N at 64–60 Ma.

For the kinematics of the Tethyan Himalaya terrane, the late Cretaceous-early Paleogene APWP is compiled from published paleomagnetic data from the Zongshan and Zongpu formations in the area of Gamba and Duila (Patzelt A et al., 1996; Yi ZY et al., 2011). However, on the exclusively reversed polarities identified from the Zongshan and the underlying Gamba Cunkou formations, Yi ZY et al. (2016) argued that the late Cretaceous carbonates in the Duela area experienced widespread remagnetization. Two later studies (Huang WT et al., 2017a, b) further reopen the discussion concerning the paleoposition of the Tethyan Himalaya. Huang WT et al. (2017a) argued for a synfolding chemical remagnetization of the Zongshan and Zongpu formations in the area of Gamba. In contrast, Yi ZY et al. (2017) reanalyzed the fold tests in the Gamba data and argued that the so-called "secondary magnetizations" were most likely acquired during early diagenesis and thus accurately reflect the pre-collisional paleoposition of the northern margin of India. More recently, a high-resolution petrographic study was carried out on carbonates from the Zongpuxi Section (the Section A of Yi ZY et al. (2011)). Along with electron microscopic observation on magnetic extracts, abundant detrital and biogenic magnetites were identified, suggesting a primary origin for the ChRMs obtained from the Zongpu Formation in the Gamba area (Zhao Q et al., 2021). The authors thus use the three paleomagnetic poles obtained from the Gamba carbonates to determine the pre-collisional kinematics of the Tethyan Himalaya terrene. The three poles include two Paleocene poles from the Lower and Upper Zongpu Formation (Yi ZY et al., 2011) and one late Cretaceous pole (about 71–65 Ma) from the Upper Zongshan Formation (Patzelt A et al., 1996).

Comparing the paleomagnetic data from the Lhasa and Himalayan terranes results in two different models as illustrated in Fig. 9. Assuming a stationary southern margin of Asia during the Late Cretaceous, the overlap of paleolatitude between the Lhasa and Tethyan Himalayan terranes did not occur until about 59–56 Ma, which corresponds to the time interval during the deposition of the Upper Zongpu Formation. In the other scenario assuming a southward shift of the Lhasa terrane, the initial collision occurred no late than about 61–59 Ma, as suggested by Yi ZY et al. (2011, 2021). This model is in good agreement with the provenance analysis in a foreland basin immediately south of the collision zone that reveals an abrupt change of provenance from India to the Gangdese belt (Asia) at about 61–59 Ma (Hu XM et al., 2015; An W et al., 2021).

In addition, two new paleomagnetic data sets were recently reported from a more distal part of the northern passive margin of India (Yuan J et al., 2021). The dataset places the Tethyan Himalaya terrane at a paleolatitude of about 19.4°S at about 75 Ma and about 13.7°N at about 61 Ma on which a two-stage collision model was proposed (Yuan J et al., 2021). Comparing the paleolatitudes resolved from the Linzhou Basin of the Lhasa terrane and from the Sandanlin Basin of the Tethyan Himalaya terrane at about 61 Ma, however, an overlap of 6° may be suggested between India

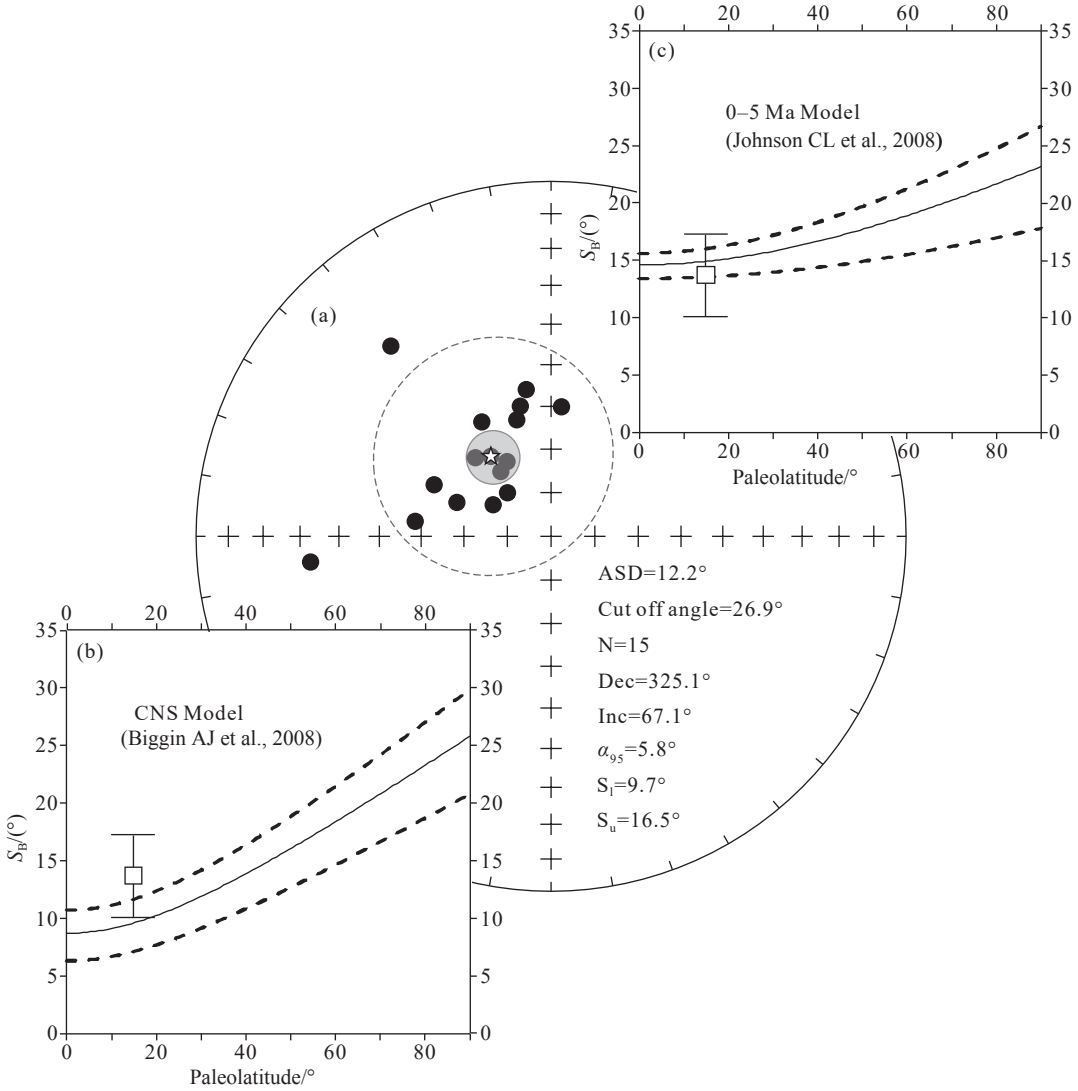

Fig. 8. Virtual geomagnetic poles (VGPs) of site-mean directions (stratigraphic coordinate) on equal-area projections. The VGP cutting-off is based on Vandamme D (1994). ASD–angular standard deviation; N–number of the VGPs; Dec–magnetic declination; Inc–magnetic declination; a_{95}–95% confidence interval of the mean paleomagnetic pole; S_B–the dispersion of VGPs and its lower (S_l) and upper (S_u) limits.

and Asia, which seemingly does not support an equatorial collision. Nevertheless, despite the uncertainty of paleomagnetism, the difference in longitude between the Linzhou and Sandanlin basins (about 6°) may be responsible for the mismatch of paleolatitude. In this case an oblique, quasi-linear structure of Asia may be suggested, as this study discuss below on the basis of a paleomagnetic analysis.

5.4. Indicator of a quasi-linear structure of the southern margin of Eurasia prior to the India-Asia collision?

A lower mantle high-velocity anomaly, highlighted by seismic tomography imaging, was interpreted as a subducted lithospheric slab of the Neo-Tethys (Van der Voo et al., 1999; Replumaz A et al., 2003, 2010, 2013). Although the present-day suture zone between India and Asia is strongly curved; the Neo-Tethyan "slab" exhibits a quasi-linear structure trending about 310° (at least to the west of about 100°E, Fig. 10c).

A detailed study of paleomagnetic declination can be used to elucidate the vertical axis rotational history of tectonically active regions (Butler RF, 1992). Several paleomagnetic studies around the western and eastern syntaxes show evidence for block rotation during the indentation of India into Eurasia. According to those models, the western side of the syntaxis rotated counterclockwise and the eastern side, oppositely (Bosboom R et al., 2014; Li SH et al., 2017 and references therein). At present, the available paleomagnetic data are insufficient to evaluate block rotations along the southern margin of Eurasia. Our paleomagnetic data obtained from the Shiquanhe and Yare basins suggest that the westernmost part of the Lhasa Terrane had a quasi-linear structure (oriented about 315°) during the Late Cretaceous. Our data are compatible with the orientation obtained via seismic tomography (Yi ZY et al., 2015, Fig. 10a).

The paleomagnetic pole obtained from the Gangdese diorite dykes, immediately north of the suture zone, reveals a counterclockwise rotation of 18°±9° since about 83 Ma. The magnitude of the rotation is similar to that calculated from red beds in the Linzhou Basin where a counterclockwise rotation of about 21° since 72–64 Ma was reported (Liang YL et al.,

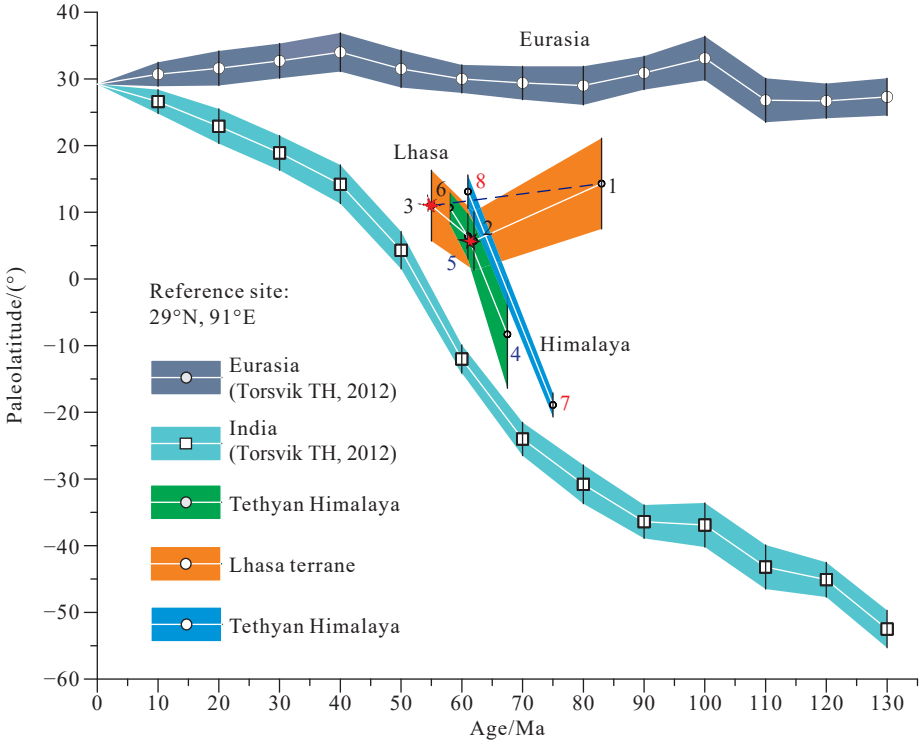

Fig. 9. Comparison of paleolatitudes of India, Eurasia, Himalayas, and Lhasa since late Cretaceous. The numbers 1, 2, 3 represent paleolatitudes for the Lhasa terrane obtained from the Gangdese pluton (dykes and country rock), Dianzhong (Yi ZY et al., 2021 compiled from Chen JS et al., 2010; 2014 and Huang WT et al., 2015) and Nianbo (Chen JS et al., 2010, 2014; Liebke U et al., 2010; Sun ZM et al., 2010) formations, whilst the numbers 4, 5, 6 indicate paleolatitudes for the Himalayas otained from the Zongshan (Yi ZY et al., 2016 revised from Patzelt A et al., 1996), lower Zongpu and upper Zongpu (Yi ZY et al., 2011) formations; Number 7 and 8 represent paleolatitude resolved from the Cailangba (Jiangzi) and Mubala (Saga) sections (Yuan J et al., 2021). See text for more explanations.

Table 2. Late Cretaceous and Paleogene paleomagnetic poles selected from the Lhasa and Himalayan terranes in this study.

Blocks	Age (Ma)	Slat. (°N)	Slong. (°E)	N(n)	Plat. (°N)	Plong. (°E)	A_{95}(or dm/dp)	Reference
Himalaya	56–59	28.3	88.5	14	71.6	277.8	2.5	Yi ZY et al., 2011
	59–62	28.3	88.5	18	67.3	266.3	3.5	Yi ZY et al., 2011
	65–71	28.3	88.5	8	51.8	257.6	8.1	Yi ZY et al., 2016 revised from Patzelt A et al., 1996
	62.5–59.2	29.3	85.3	86	74	278.5	2.5	Yuan J et al., 2021
	76.2–74.0	28.9	89.2	127	40.8	256.3	1.8	Yuan J et al., 2021
Lhasa	55	30.0	91.1	46	70.9	249.8	5.3	Combined from Chen JS et al., 2010, 2014; Liebke U et al., 2010 and Sun ZM et al., 2010
	62	30.0	91.1	35	65.8	254.1	4.4	Yi ZY et al., 2021
	83	29.5	90.0	15	67.1	325.1	6.8	this study

2017). These studies suggest that the southern margin of Eurasia (near Lhasa) has rotated 18–20° counterclockwisely since the late Cretaceous. Moreover, the mean strike of the dykes in this study is about 290°, then if the authors correct for the counterclockwise rotation of about 18°, the original strike of the dykes is 308° (Fig. 10b).

Ma XX et al. (2017) concluded on the basis of petrologic, geochronologic, geochemical and isotopic studies of the same suite of plutonic rocks, the dykes within the Gangdese arc were generated in an intra-arc extensional setting. If this scenario is correct, the dykes should theoretically parallel the subduction zone (the trench) along the Gandese arc (Ma XX et al., 2017). The initial strike of the dykes hence suggests that the strike of the Gandese arc, such as the southern margin of Asia near Lhasa, was trending about 310° during late Cretaceous time (at about 83 Ma). That agrees well with the strike of the active margin during the Cretaceous as indicated by seismic tomography and hence is an indicator of a quasi-linear structure of the southern margin of Eurasia prior to the India-Asia collision (Fig. 10c).

6. Conclusions

Our paleomagnetic study of the late Cretaceous diorite dykes and granodiorite host yielded a paleomagnetic pole at 67.1°N, 325.1°E with A_{95} = 5.8° for the Gangdese batholith. A comparison between out pole and coeval poles from the eastern part of the Lhasa Terrane, Tethyan Himalaya and Asia, this study reach the following conclusions:

(i) The eastern segment of the Lhasa Terrane was located at about 14°N during the Late Cretaceous (about 83 Ma). Our result is consistent with a re-evaluation of coeval

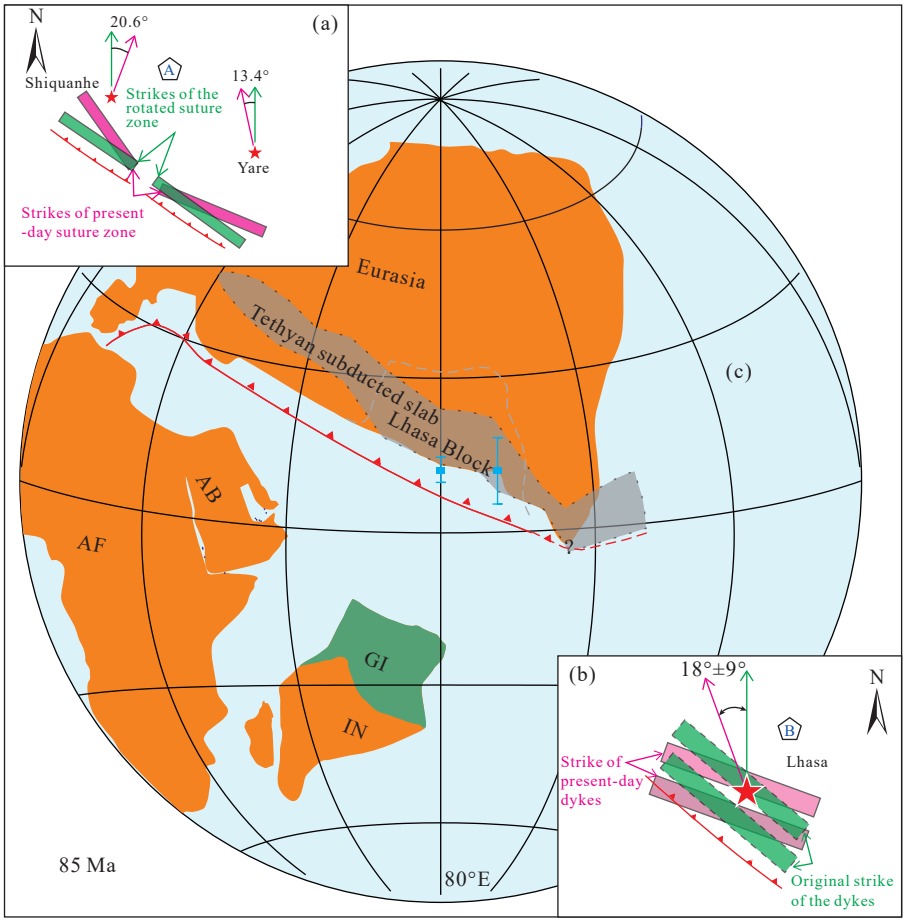

Fig. 10. (a) Reconstructions of the southern margin of Eurasia prior to the India-Asia collison (about 85 Ma). Precollisional positions of the southern margin of Asia in its western and eastern segments are constrained by paleomagnetic data from Yi ZY et al. (2015) and this study, respectively. The precollisional strike of the southern margin of Asia at about 80°E (b) is restored on paleomagnetic data obtained from the late Cretaceous volcanic rocks in the Shiquanhe and Yare basins according to Yi ZY et al. (2015) ; the precollisional strike of the southern margin of Asia at about 90°E (c) is inferred from the original strike of the late Cretaceous dykes (this study) in consideraion that the dykes were generated by an arc-paralelled extension caused by Neo-Tethys subduction in the late Cretaceous (Ma XX et al., 2017). solid lines and arrows in green in (b) and (c) were restored by aligning the documented declinations (solid lines and arrows in green) to the geographic north; Eurasia, Africa, Arabia and India in (a) are positioned in accordance with the APW path of Torsvik TH et al. (2012); the Neo-Tethyan subducted slab is constructed according to Van der Voo et al. (1999). Abbreviations: IN–India; GI–"Greater India"; AB–Arabia; AF–Afrian. The "Greater India" of about 1500 km is defined according to Yi ZY et al. (2011).

paleomagnetic data from the Lhasa Terrane and corresponds to an in-between position of the Lhasa terrane during about 130–60 Ma.

(ii) Paleolatitudinal plots of the Lhasa and Himalaya indicate that the two terranes were separated at about 83 Ma but in close proximity during about 61–59 Ma, suggesting an initial collision between India and Asia during this interval.

(iii) The mean magnetic declination of the ChRMs reveals a significant counterclockwise rotation of 18°±9° for the sampling location relative to the north since about 83 Ma. In the light of tectonic setting of the dykes, the strike of the southern margin of Asia near Lhasa is restored to about 310° and supports a quasi-linear margin between Eurasia and India during the Cretaceous.

Acknowledgments

Yan-long Wang, Shao-yuan Ma and Drs, Xiao-dong Tan, Yu-lin Han are acknowledged for laboratorial assistance. This work was financially supported by the National Science Foundation of China (92055205, 41672223) and the start-up funding from Sun Yat-sen University (74110-18841244).

CRediT authorship contribution statement

Zhi-yu Yi and Si-lin Yang conceived of the presented idea. Zhi-yu Yi, Si-lin Yang, Joseph Meert, Xu-xuan Ma prepared the manuscript. Zhi-yu Yi, Si-lin Yang carried out the experiment. Zhi-yu Yi, Si-lin Yang, Xu-xuan Ma contributed to sample preparation. All authors discussed the results and contributed to the final manuscript.

Declaration of competing interest

The authors declare no conflicts of interest.

References

Achache J, Courtillot V, Xiu ZY. 1991. Paleogeographic and Tectonic

evolution of southern Xizang (Tibet) since middle Cretaceous time: new paleomagnetic data and synthesis. Geology of the Himalayas-Papers on Geophysics, Geological Printing House, Beijing, 201–244.

Achache J, Courtillot V, Xiu ZY. 1984. Paleogeographic and tectonic evolution of southern Tibet since middle Cretaceous time-new paleomagnetic data and synthesis. Journal of Geophysical Research, 89(b12), 10311–10339. doi: 10.1029/jb089ib12p10311.

Aitchison JC, Ali JR, Davis AM. 2007. When and where did India and Asia collide? Journal of Geophysical Research, 112 (B05423), 1–12. doi:10.1029/2006jb004706.

An W, Hu X, Garzanti E, Wang JG, Liu Q. 2021. New precise dating of the India-Asia collision in the Tibetan Himalaya at 61 Ma. Geophysical Research Letters, 48. e2020GL090641. DOI: 10.1029/2020GL090641.

Belica ME, Piispa EJ, Meert JG, Pesonen LJ, Plado J, Pandit MK, Kamenov GD, Celestino M. 2014. Paleoproterozoic mafic dyke swarms from the Dharwar craton; paleomagnetic poles for India from 2. 37 to 1. 88 Ga and rethinking the Columbia supercontinent. Precambrian Research, 244, 100–122. doi: 10.1016/j.precamres.2013.12.005.

Biggin AJ, van Hinsbergen DJJ, Langereis CG, Straathof GB, and Deenen MHL. 2008. Geomagnetic secular variation in the Cretaceous Normal Superchron and in the Jurassic. Physics of the Earth and Planetary Interiors, 169(1–4), 3–19. doi:10.1016/j.pepi.2008.07.004.

Borradaile GJ, and Jackson M. 2004. Anisotropy of magnetic susceptibility (AMS): magnetic petrofabrics of deformed rocks. Geological Society, London, Special Publications, 238(1), 299–360. doi:10.1144/GSL.SP.2004.238.01.18.

Bosboom R, Dupont-Nivet G, Huang W, Yang W, Guo Z. 2014. Oligocene clockwise rotations along the eastern Pamir: Tectonic and paleogeographic implications. Tectonics, 33(2), 53–66. doi: 10.1002/2013TC003388.

Buchan KL, and Halls HC. 1990. Paleomagnetism of proterozoic mafic Dyke Swarms of the Canadian shield. Mafic Dykes and Emplacement Mechanisms. Rotterdam, Balkema, 209–230. doi: 10.1007/BF02879661.

Butler RF. 1992. Paleomagnetism: Magnetic Domains to Geologic Terranes (Vol. 319). Boston, Blackwell Scientific Publications. 205-222.

Cao Y, Sun Z, Li H, Pei J, Jiang W, Xu W, Zhao L, Wang L, Li C, Ye X, Zhang L. 2017. New Late Cretaceous paleomagnetic data from volcanic rocks and red beds from the Lhasa terrane and its implications for the paleolatitude of the southern margin of Asia prior to the collision with India. Gondwana Research, 41, 337–351. doi: 10.1016/j.gr.2015.11.006.

Carvallo C, Dunlop DJ, Özdemir Ö. 2005. Experimental comparison of FORC and remanent Preisach diagrams. Geophysical Journal International, 162(3), 747–754. doi: 10.1111/j.1365-246x.2005.02688.x.

Chen JS, Huang BC, Sun LS. 2010. New constraints to the onset of the India-Asia collision: Paleomagnetic reconnaissance on the Linzizong Group in the Lhasa Terrane, China. Tectonophysics, 489(1–4), 189–209. doi: 10.1016/j.tecto.2010.04.024.

Chen JS, Huang BC, Yi ZY, Yang LK, Chen LW. 2014. Paleomagnetic and $^{40}Ar/^{39}Ar$ geochronological results from the Linzizong Group, Linzhou Basin, Lhasa Terrane, Tibet: implications to Paleogene paleolatitude and onset of the India-Asia collision. Journal of Asian Earth Sciences, 96, 162–177. doi: 10.1016/j.jseaes.2014.09.007.

Chen Y, Cogné JP, Courtillot V, Tapponnier P, Zhu XY, 1993. Cretaceous Paleomagnetic Results from Western Tibet and Tectonic Implications. Journal of Geophysical Research: Solid Earth, 98(B10), 17981–17999. doi:10.1029/93jb01006.

Chen Y, Xu B, Zhan S, Li YG. 2004. First mid-Neoproterozoic paleomagnetic results from the Tarim Basin (NW China) and their geodynamic implications. Precambrian Research, 133(3), 271–281. doi: 10.1016/j.precamres.2004.05.002.

Chung SL, Chu MF, Zhang YQ, Xie YW, Lo CH, Lee TY, Lan CY, Li XH, Zhang Q, Wang YZ. 2005. Tibetan tectonic evolution inferred from spatial and temporal variations in post-collisional magmatism. Earth-Science Reviews, 68, 173–196. doi: 10.1016/J.EARSCIREV.2004.05.001.

Day R, Fuller M, and Schmidt VA. 1977. Hysteresis properties of titanomagnetites: grain-size and compositional dependence. Physics of the Earth and planetary interiors, 13(4), 260–267. doi: 10.1016/0031-9201(77)90108-X.

Dunlop DJ. 2002. Theory and application of the Day plot (Mrs/Ms versus Hcr/Hc) 1. Theoretical curves and tests using titanomagnetite data. Journal of Geophysical Research: Solid Earth, 107(B3), 2057–2061. doi: 10.1029/2001JB000487.

Enkin RJ, Chen Y, Courtillot V, Besse J, Xing L, Zhang Z, Zhuang Z, Zhang J. 1991. A Cretaceous pole from south China, and the Mesozoic hairpin turn of the Eurasian apparent polar wander path. Journal of Geophysical Research:Solid Earth, 96(B3), 4007–4027. doi: 10.1029/90JB01904.

Fisher R. 1953. Dispersion on a Sphere. London:Proceedings of the Royal Society, 295–305. doi: 10.2307/99186.

Guo L, Zhang HF, Harris N, Pan FB, Xu WC. 2011. Origin and evolution of multi-stage felsic melts in eastern Gangdese belt: constraints from U-Pb zircon dating and Hf isotopic composition. Lithos, 127, 54–67. doi: 10.1016/j.lithos.2011.08.005.

Guo LS, Liu YL, Liu SW, Cawood PA, Wang ZH, Liu HF. 2013. Petrogenesis of Early to Middle Jurassic granitoid rocks from the Gangdese belt, Southern Tibet: implications for early history of the Neo-Tethys. Lithos, 179, 320–333. doi: 10.1016/j.lithos.2013.06.011.

Halls HC. 1978. The use of converging remagnetization circles in palaeomagnetism. Physics of the Earth and Planetary Interiors, 16(1), 1–11. doi: 10.1016/0031-9201(78)90095-X.

Halls HC, Li J, Davis D, Hou G, Zhang B, Qian X. 2000. A precisely dated Proterozoic palaeomagnetic pole from the North China craton, and its relevance to palaeocontinental reconstruction. Geophysical Journal International, 143(1), 185–203. doi: 10.1046/j.1365-246x.2000.00231.x.

Huang WT, Dupont-Nivet G, Lippert PC, van Hinsbergen DJ, Hallot E. 2013. Inclination shallowing in Eocene Linzizong sedimentary rocks from Southern Tibet: Correction, possible causes and implications for reconstructing the India –Asia collision. Geophysical Journal International, 194, 1390–1411. doi: 10.1093/gji/ggt188.

Huang WT, Dupont‐Nivet G, Lippert PC, Hinsbergen DJ, Dekkers MJ, Guo ZJ, Waldrip R, Li XC, Zhang XR, Liu DD, Kapp P. 2015. Can a primary remanence be retrieved from partially remagnetized Eocence volcanic rocks in the Nanmulin Basin (southern Tibet) to date the India-Asia collision? Journal of Geophysical Research: Solid Earth, 120(1), 42–66. doi: 10.1002/2014JB011599.

Huang WT, Lippert PC, Jackson MJ, Dekkers MJ, Zhang Y, Li J, Guo ZJ, Kapp P, Hinsbergen DJ. 2017a. Remagnetization of the Paleogene Tibetan Himalayan carbonate rocks in the Gamba area: Implications for reconstructing the lower plate in the India-Asia collision. Journal of Geophysical Research:Solid Earth, 122(2), 808–825. doi: 10.1002/2016JB013662.

Huang WT, Lippert PC, Zhang Y, Jackson MJ, Dekkers MJ, Li J, Hu XM, Zhang B, Guo ZJ, Hinsbergen DJ. 2017b. Remagnetization of carbonate rocks in southern Tibet: Perspectives from rock magnetic and petrographic investigations. Journal of Geophysical Research: Solid Earth, 122(4), 2434–2456. doi: 10.1002/2017JB013987.

Ji WQ, Wu FY, Chung SL, Li JX, Liu CZ. 2009. Zircon U-Pb geochronology and Hf isotopic constraints on petrogenesis of the Gangdese batholith, southern Tibet. Chemical Geology, 262,

229–245. doi: 10.1016/J.CHEMGEO.2009.01.020.

Johnson CL, Constable CG, Tauxe L, Barendregt R, Brown LL, Coe RS. 2008. Recent investigations of the 0-– 5 Ma geomagnetic field recorded by lava flows. Geochemistry Geophysics Geosystems, 9(4), Q04032. doi: 10.1029/2007GC001696.

Kirschvink JL. 1980. The least-squares line and plane and the analysis of Paleomagnetic data. Geophysical Journal of the Royal Astronomical Society, 62(3), 699–718. doi: 10.1111/j.1365-246X.1980.tb02601.x.

Li S, Advokaat EL, van Hinsbergen DJ, Koymans M, Deng C, Zhu R. 2017. Paleomagnetic constraints on the Mesozoic-Cenozoic paleolatitudinal and rotational history of Indochina and South China: Review and updated kinematic reconstruction. Earth-Science Reviews, 2017, S0012825217300247. doi: 10.1016/j.earscirev. 2017.05.007.

Liang YL, Huang BC, Yi ZY, Zhang Y, Yan YG, Zhang DH. 2017. Reconnaissance of pre-collisional paleolatitudes of the southern margin of Eurasia: New paleomagnetic results from Upper Cretaceous red beds in the Linzhou Basin, Tibet. Chinese Journal of Geophysics, 60(5), 1811–1824. doi: 10.6038/cjg20170517.

Liebke U, Appel E, Ding L, Neumann U, Antolin B, Xu Q. 2010. Position of the Lhasa terrane prior to India–Asia collision derived from palaeomagnetic inclinations of 53 Ma old dykes of the Linzhou Basin: constraints on the age of collision and post-collisional shortening within the Tibetan Plateau. Geophysical Journal International, 182(3), 1199–1215. doi: 10.1111/j.1365-246X.2010. 04698.x.

Lin J, Watts DR. 1988. Palaeomagnetic results from the Tibetan Plateau. Philosophical Transactions of the Royal Society A, 327, 239–262. doi: 10.1098/rsta.1988.0128.

Liu Z, and Buck WR. 2021. Magmatic sill formation during dike opening. Geology, 50(4), 407–411. doi: 10.1016/j.jvolgeores.2014. 05.018.

Lippert PC, van Hinsbergen DJJ, Dupont-Nivet G. 2014. The early Cretaceous to present latitude of the central Lhasa-plano (Tibet): A paleomagnetic synthesis with implications for Cenozoic tectonics, paleogeography and climate of Asia, in: Nie JS. , Hoke GD. and Horton BK. (editors), Geological Society of America Special Paper: Towards an improved understanding of uplift mechanisms and the elevation history of the Tibetan plateau: Boulder, Co, Geological Society of America, p. 1–21,doi: 10.1130.2014.2507(01).

Ma L, Wang Q, Wyman DA, Li ZX, Jiang ZQ, Yang JH, Gou GN, Guo HF. 2013. Late Cretaceous (100– 89 Ma) magnesian charnockites with adakitic affinities in the Milin area, eastern Gangdese: partial melting of subducted oceanic crust and implications for crustal growth in southern Tibet. Lithos, 175–176, 315–332. doi: 10.1016/ j.lithos.2013.04.006.

Ma X, Xu Z, and Meert JG. 2017. Syn-convergence extension in the southern Lhasa terrane: Evidence from late Cretaceous adakitic granodiorite and coeval gabbroic-dioritic dykes. Journal of Geodynamics, 110, 12–30. doi: 10.1016/j.jog.2017.07.004.

Ma Y, Yang T, Bian W, Jin J, Wang Q, Zhang S, Wu H, Li H, Cao L, Yuan H, and Ding J. 2017. Paleomagnetic and geochronologic results of latest Cretaceous lava flows from the Lhasa Terrane and their tectonic implications. Journal of Geophysical Research:Solid Earth, 122, 8786–8809. doi: 10.1002/2017JB014743.

Ma Y, Wang Q, Yang T, Ou Q, Zhang X, Dan W, Zhang S, Wu H, Li, Cao L, Wang J. 2022. Location of the Lhasa terrane in the Late Cretaceous and its implications for crustal deformation. Palaeogeography, Palaeoclimatology, Palaeoecology, 588, 110821. doi: 10.1016/j.palaeo.2021.110821.

McFadden PL, McElhinny MW. 1990. Classification of the reversal test in palaeomagnetism. Geophysical Journal International, 103(3), 725–729. doi: 10.1111/j.1365-246X.1990.tb05683.x.

Morris A, Maffione M. 2016. Is the Troodos ophiolite (Cyprus) a complete, transform fault –bounded Neotethyan ridge segment? Geology, 44(3), 199–202. doi: 10.1130/G37529.1.

Muxworthy AR, Roberts AP. 2007. First-order reversal curve (FORC) diagrams. in Encyclopedia of Geomagnetism and Paleomagnetism, edited by D. Gubbins, and E. Herrero-Bervera, Springer, New York. doi: 10.1007/978-1-4020-4423-6_99.

Najman Y, Appel E, Boudagher‐Fadel M, Bown P, Carter A, Garzanti E, Godin L, Han J, Liebke U, Oliver G, Parrish R. 2010. Timing of India-Asia collision: Geological, biostratigraphic, and palaeomagnetic constraints. Journal of Geophysical Research: Solid Earth, 115(B12). doi: 10.1029/2010jb007673.

Patriat P, Achache J. 1984. India –Eurasia collision chronology has implications for crustal shortening and driving mechanism of plates. Nature, 311(5987), 615–621. doi: 10.1038/311615a0.

Patzelt A, Li H, Wang J, Appel E. 1996. Palaeomagnetism of Cretaceous to Tertiary sediments from southern Tibet: evidence for the extent of the northern margin of India prior to the collision with Eurasia. Tectonophysics, 259(4), 259–284. doi: 10.1016/0040-1951(95) 00181-6.

Pozzi JP, Westphal M, Zhou YX, Xing LS, Chen XY, 1982. Position of the Lhasa Block, South Tibet, during the Late Cretaceous. Nature, 297(5864), 319–321. doi: 10.1038/297319a0.

Replumaz A, Negredo AM, Villasenor A, Stéphane G. 2010. Indian continental subduction and slab break-off during Tertiary collision. Terra Nova, 22(4), 290–296. doi: 10.1111/j.1365-3121.2010.00945.x.

Replumaz A, Tapponnier P. 2003. Reconstruction of the deformed collision zone between India and Asia by backward motion of lithospheric blocks. Journal of Geophysical Research: Solid Earth, 108(B6), 1978–2012. doi: 10.1029 /2001jb000661.

Replumaz A, Guillot S, Villaseñor A, Negredo AM. 2013. Amount of Asian lithospheric mantle subducted during the India/Asia collision. Gondwana Research, 24(3 –4), 936–945. doi: 10.1016/j.gr.2012. 07.019.

Roberts AP, Pike CR, Verosub KL. 2000. First-order reversal curve diagrams: A new tool for characterizing the magnetic properties of natural samples. Journal of Geophysical Research:Solid Earth, 105(B12), 28461–28475. doi: 10.1046/j.0956-540x.2001.01419.x.

Schärer U, Allègre CJ. 1984. U-Pb geochronology of the Gangdese (Transhimalaya) plutonism in the Lhasa-Xigaze region, Tibet. Earth and Planetary Science Letters 63, 423–432. doi: 10.1016/0012-821X(84)90190-0.

Sun Z, Pei J, Li H, Xu W, Jiang W, Zhu Z, Wang X, Yang Z. 2012. Palaeomagnetism of late Cretaceous sediments from southern Tibet: Evidence for the consistent palaeolatitudes of the southern margin of Eurasia prior to the collision with India. Gondwana Research, 21(1), 53–63. doi: 10.1016/j.gr.2011.08.003.

Sun Z, Jiang W, Li H, Pei J, Zhu Z. 2010. New paleomagnetic results of Paleocene volcanic rocks from the Lhasa block: Tectonic implications for the collision of India and Asia. Tectonophysics, 490(3–4), 257–266. doi: 10.1016/j.tecto.2010.05.011.

Tan X, Kodama KP. 2002. Magnetic anisotropy and paleomagnetic inclination shallowing in red beds: Evidence from the Mississippian Mauch Chunk Formation, Pennsylvania. Journal of Geophysical Research, 107(B11), 2311. doi: 10.1029/2001JB001636.

Tan X, Gilder S, Kodama KP, Jiang W, Han Y, Zhang H, Xu H, Zhou D. 2010. New paleomagnetic results from the Lhasa block: Revised estimation of latitudinal shortening across Tibet and implications for dating the India-Asia collision. Earth and Planetary Science Letters, 293(3–4), 396–404. doi: 10.1016/j.epsl.2010.03.013.

Tauxe L. 2005. Inclination flattening and the geocentric axial dipole hypothesis. Earth and Planetary Science Letters, 233(3–4), 247–261. doi: 10.1016/j.epsl.2005.01.027.

Tong Y, Yang Z, Pei J, Wang H, Xu Y, Pu Z. 2017. Paleomagnetism of the Upper Cretaceous red-beds from the eastern edge of the Lhasa

Terrane: New constraints on the onset of the India-Eurasia collision and latitudinal crustal shortening in southern Eurasia. Gondwana Research, 48, 86–100. doi: 10.1016/j.gr.2017.04.018.

Tong Y, Yang Z, Pei J, Li J, Jin S, Hou L, Sun X, Zhang Z. 2022. New Late Cretaceous paleomagnetic results from the Lhasa terrane and their implications for the suturing of India and Eurasia and the closure of the Neo-Tethys Ocean. Bulletin, 134(11–12), 3242–3257. https://doi.org/10.1130/B36310.1.

Torsvik TH, Van der Voo R, Preeden U, Mac Niocaill C, Steinberger B, Doubrovine PV, van Hinsbergen DJ, Domeier M, Gaina C, Tohver E. Meert JG. 2012. Phanerozoic polar wander, palaeogeography and dynamics. Earth-Science Reviews, 114(3), 325–368. doi: 10.1016/j.earscirev.2012.06.007.

Van der Voo R, Spakman W, Bijwaard H. 1999. Tethyan subducted slabs under India. Earth and Planetary Science Letters, 171(1), 7–20. doi: 10.1016/s0012-821x(99)00131-4.

van Hinsbergen DJJ, Lippert PC, Dupont-Nivet G, McQuarrie N, Doubrovine PV, Spakman W, Torsvik TH. 2012. Greater India Basin hypothesis and a two-stage Cenozoic collision between India and Asia. Proceedings of the National Academy of Sciences, 109(20), 7659–7664. doi: 10.1073/pnas.1117262109.

Vandamme D. 1994. A new method to determine paleosecular variation. Physics of the Earth and Planetary Interiors, 85(1–2), 131–142. doi: 10.1016/0031-9201(94)90012-4.

Wang C, Ding L, Zhang LY, Kapp P, Pullen A, Yue YH. 2016. Petrogenesis of Middle –Late Triassic volcanic rocks from the Gangdese belt, southern Lhasa terrane: Implications for early subduction of Neo-Tethyan oceanic lithosphere. Lithos, 262, 320–333. doi: 10.1016/j.lithos.2016.07.021.

Wang JG, Hu X, Garzanti E, Boudagher-Fadel MK, Liu ZC, Li J, Wu FY. 2020. From extension to tectonic inversion: Mid-Cretaceous onset of Andean-type orogeny in the Lhasa block and early topographic growth of Tibet. GSA Bulletin, 132(11–12): 2432–2454. doi: 10.1130/B35314.1.

Westphal M, Pozzi JP. 1983. Paleomagnetic and Plate Tectonic Constraints on the Movement of Tibet. Tectonophysics, 98(1–2), 1–10. doi: 10.1016/0040-1951(83)90207-X.

Xu WC, Zhang HF, Luo BJ, Guo L, Yang H. 2015. Adakite-like geochemical signature produced by amphibole-dominated fractionation of arc magmas: An example from the Late Cretaceous magmatism in Gangdese belt, south Tibet. Lithos, 232, 197–210. doi: 10.1016/j.lithos.2015.07.001.

Yi ZY, Huang BC, Chen JS, Chen LW, Wang HL. 2011. Paleomagnetism of early Paleogene marine sediments in southern Tibet, China: Implications to onset of the India-Asia collision and size of Greater India. Earth and Planetary Science Letters, 309(1–2), 153–165. doi: 10.1016/j.epsl.2011.07.001.

Yi ZY, Huang B, Yang L, Tang X, Yan Y, Qiao Q, Zhao J, Chen L. 2015. A quasi‐linear structure of the southern margin of Eurasia prior to the India‐Asia collision: First paleomagnetic constraints from Upper Cretaceous volcanic rocks near the western syntaxis of Tibet. Tectonics, 34(7), 1431–1451. doi: 10.1002/2014TC003571.

Yi ZY, Liang Y, Zhao J, Yan Y, Chen L, Tang X. 2016. Paleogeography of the Northern Margin of India continent prior to its collision: An investigation of the Late Cretaceous limestones in South Tibet. Acta Geologica Sinica, 90(11), 3282–3292.

Yi ZY, Appel E, Huang B. 2017. Comment on “Remagnetization of the Paleogene Tibetan Himalayan carbonate rocks in the Gamba area: Implications for reconstructing the lower plate in the India‐Asia collision” by Huang et al. Journal of Geophysical Research:Solid Earth, 122(7), 4852–4858. doi: 10.1002/2017JB014353.

Yi ZY, Wang T, Meert JG, Zhao Q, Liu Y. 2021. An initial collision of India and Asia in the equatorial humid belt. Geophysical Research Letters, 48(9), e2021GL093408. doi: 10.1029/2021GL093408.

Yuan J, Yang Z, Deng C, Krijgsman W, Hu X, Li S, Shen Z, Qin H, An W, He H, Ding L. 2021. Rapid drift of the Tethyan Himalaya terrane before two-stage India-Asia collision. National Science Review, 8(7), 173. doi: 10.1093/nsr/nwaa173.

Zhang X, Chung SL, Lai YM, Ghani AA, Murtadha S, Lee HY, Hsu CC. 2019. A 6000-km-long Neo-Tethyan arc system with coherent magmatic flare-ups and lulls in South Asia. Geology, 47(6), 573–576. doi: 10.1130/G46172.1.

Zhao Q, Huang B, Yi Z, Xue P. 2021. High-Resolution PetrographicEvidence Confirming Detrital and Biogenic Magnetites as Remanence Carriersfor Zongpu Carbonates in the Gamba Area, South Tibet. Earth Science Frontiers 9, 713469. doi: 10.3389/feart.2021.713469.

Zhou S, Mo X, Dong G, Zhao Z, Qiu R, Guo T, Wang L. 2004. Ar-40/Ar-39 geochronology of Cenozoic Linzizong volcanic rocks from Linzhou Basin, Tibet, China, and their geological implications. Chinese Science Bulletin, 49, 1970–1979. doi: 10.1360/03wd0511.

Zhu DC, Zhao ZD, Niu YL, Dilek Y, Hou ZQ, Mo XX. 2013. The origin and pre-Cenozoic evolution of the Tibetan plateau. Gondwana Research, 23, 1429–1454. doi: 10.1016/j.gr.2012.02.002.

Zhu R, Laj C, and Mazaud A. 1994. The Matuyama-Brunhes and Upper Jaramillo transitions recorded in a loess section at Weinan, north-central China. Earth and Planetary Science Letters, 125(1-4), 143–158. doi: 10.1016/0012-821X(94)90212-7.

Zhu XY, Liu C, Ye SJ, Lin JL. 1977. Remanence of red beds from Linzhou, Xizang and the northward movement of the Indian plate. Chinese Journal of Geology, 1, 44–51.

Zhu ZW, Zhu XY, Zhang YM. 1981. Paleomagnetic observation in Xizang and continental-drift. Acta Geophysica Sinica, 24(1), 40–49.

Zijderveld JDA. 1967. AC demagnetization of rocks: Analysis of results. Methods in Palaeomagnetism, 254–286. doi: 10.1016/B978-1-4832-2894-5.50049-5.